Fiber Pathway Pathology, Synapse Loss and Decline of Cortical Function in Schizophrenia

Max R. Bennett[1,2]*, Les Farnell[2,3], William G. Gibson[2,3]

1 The Brain and Mind Research Institute, University of Sydney, Sydney, NSW, Australia, 2 The Centre for Mathematical Biology, University of Sydney, Sydney, NSW, Australia, 3 The School of Mathematics and Statistics, University of Sydney, Sydney, NSW, Australia

Abstract

A quantitative cortical model is developed, based on both computational and simulation approaches, which relates measured changes in cortical activity of gray matter with changes in the integrity of longitudinal fiber pathways. The model consists of modules of up to 5,000 neurons each, 80% excitatory and 20% inhibitory, with these having different degrees of synaptic connectiveness both within a module as well as between modules. It is shown that if the inter-modular synaptic connections are reduced to zero while maintaining the intra-modular synaptic connections constant, then activity in the modules is reduced by about 50%. This agrees with experimental observations in which cortical electrical activity in a region of interest, measured using the rate of oxidative glucose metabolism ($CMR_{glc(ox)}$), is reduced by about 50% when the cortical region is isolated, either by surgical means or by transient cold block. There is also a 50% decrease in measured cortical activity following inactivation of the nucleus of Meynert and the intra-laminar nuclei of the thalamus, which arise either following appropriate lesions or in sleep. This occurs in the model if the inter-modular synaptic connections require input from these nuclei in order to function. In schizophrenia there is a 24% decrease in functional anisotropy of longitudinal fasciculi accompanied by a 7% decrease in cortical activity ($CMR_{glc(ox)}$).The cortical model predicts this, namely for a 24% decrease in the functioning of the inter-modular connections, either through the complete loss of 24% of axons subserving the connections or due to such a decrease in the efficacy of all the inter-modular connections, there will be about a 7% decrease in the activity of the modules. This work suggests that deterioration of longitudinal fasciculi in schizophrenia explains the loss of activity in the gray matter.

Competing Interests: The authors have declared that no competing interests exist.

* E-mail: max.bennett@sydney.edu.au

Introduction

Goldman-Rakic [1] was the first to highlight the possible dysfunction of major fiber pathways in the cortex of those suffering from schizophrenia. Such impairments in white matter have now been identified (for a meta-analysis of studies, see [2] and explained in terms of their impact on cognition [3]. Particular emphasis has been placed on the superior longitudinal fasciculus (SLF), a major fiber pathway that connects the supramarginal gyrus of the parietal lobe with the middle frontal gyrus/ dorsolateral prefrontal cortex [4,5]. The reason for this is that the posterior parietal and frontal cortices form a network [6] which supports working memory [7,8,9] and matures as fiber pathways between these parts of the cortex mature [10]. The parietal and frontal components of this network show pathological changes in schizophrenia, both indicated by loss of gray matter [11,12] and white matter [13–18]; for a recent review, see [19]. The fronto-parietal network receives major inputs from the thalamic intralaminar nuclei and the basal nuclei whose integrity is necessary for the normal functioning of the network. [20,21].

For over a decade functional magnetic resonance imaging (fMRI) has revealed irregularities in the activity of the fronto-parietal network in schizophrenia [22–25]. A number of different techniques indicate subnormal connectivity between fronto-

parietal and fronto-temporal regions [24–28]. Consistent with these observations, diffusion tensor imaging (DTI) has revealed reduced fractional anisotropy in the SLF, the main pathway between frontal and parietal cortex, as well as in the cingulum fasciculus, the pathway subserving the fronto-temporal connection [29]. Indeed the extent of fractional anisotropy of the superior longitudinal fasciculus is correlated with decreases in working memory in schizophrenia patients, a capacity that depends on the integrity of the fronto-parietal network [19,29]. Furthermore, disturbances in the integrity of the SLF in schizophrenia are indicated by transcranial magnetic stimulation (TMS) of the parietal-motor pathway [30].

Very extensive studies have been made of activity in the different components of the fronto-parietal network, using the rate of oxidative glucose metabolism ($CMR_{glc(ox)}$) as a measure of the activity, based on the very close quantitative relationship between synaptic and action potential firing in a cortical area of interest and $CMR_{glc(ox)}$ in that area [31]. Decreases in $CMR_{glc(ox)}$ have been noted in the fronto-parietal network of patients with schizophrenia compared with controls (see, for example, [32]. The present work seeks to determine whether the observed changes in functioning of the fronto-parietal network, measured with $CMR_{glc(ox)}$, can be explained in terms of the changes in integrity of the longitudinal fascicules subserving the network.

Methods

We use two different theoretical models in order to investigate the effects of changing synaptic connectiveness in the cortical model (Figure 1). The first (Model 1) is a simple firing-rate model; however, in many cases it can provide an adequate description of network activity (see comments and references to earlier work in [33]. The second (Model 2) uses integrate-and-fire neurons; these have been extensively employed in theoretical investigations of network behaviour [34]. The principal reason for using two models was to provide some evidence that the main theoretical results reported here are not dependent on the particular neural network model employed. The models are rather different and it is not the purpose of the present research to do a detailed comparison of them, but rather to show that they give similar results in the context of the present investigation. Specifically, the models are used to compute the decrease in neuronal activity as the coupling between subsets of interconnected neurons is decreased.

Model 1

In this model, the neurons are described by firing rates, not by action potentials. We follow the formulation of [35].

The network consists of $\mathcal{N}$ interconnected neurons, with no distinction being made between excitatory and inhibitory ones. Neuron i is characterized by an activation variable x_i satisfying

$$\tau dx_i/dt = -x_i + g \sum_{j=1}^{N} J_{ij} r_j, \qquad (1)$$

where τ is the membrane time constant, J_{ij} describes the connection from neuron j to neuron i and g is a parameter controlling the strength of the synaptic connections. The quantities
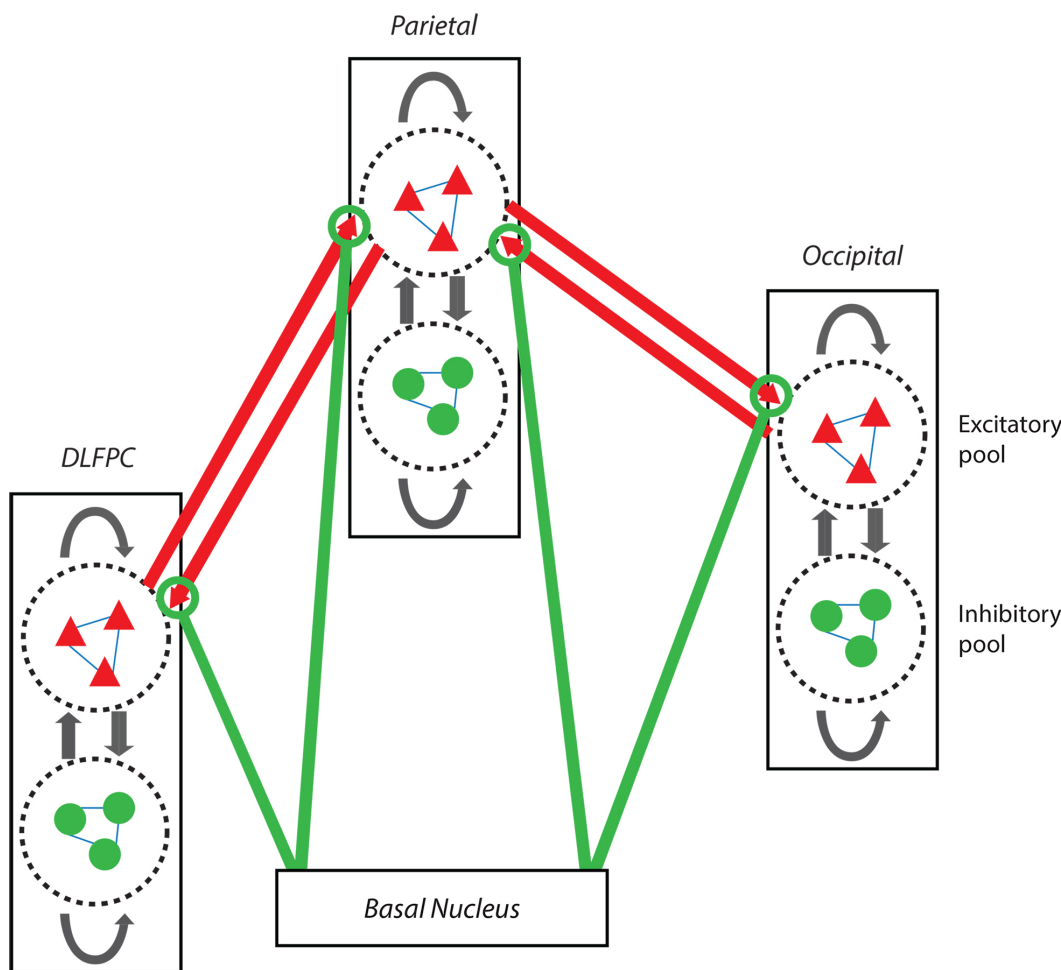

Figure 1. Model of a modular network such as that connecting the dorso-lateral prefrontal (DLPC)/parietal/occipital cortical modules. However, these are only given as being representative of typical cortical regions, and in the computations each module (indicated by a rectangle) contains an identical neural network with N neurons, 20% inhibitory (green), 80% excitatory (red), each connected to other neurons with connection strength A_k for excitatory neurons and B_k for inhibitory neurons. The arrows in the rectangles indicate that excitatory neurons are connected with each other and to inhibitory neurons, as well as projecting to other modules (long red arrows). Likewise, other arrows in the rectangles indicate that inhibitory neurons are connected with each other and to excitatory neurons. The lower module represents projections to the upper modules from the basal nuclei (magnocellularis in rat and Meynert in humans) and the non-specific intralaminar nuclei of the thalamus (green arrows). These are taken here to specifically change the efficacy of transmission of associational synapses in the modules (the green lines end in circles, taken to indicate their synapsing on synaptic endings between modules (red-arrow heads). This figure is for Model 2 and the mathematical theory is given under Methods.
doi:10.1371/journal.pone.0060518.g001

J_{ij} are chosen independently and randomly from a Gaussian distribution with mean 0 and variance 1/N; hence about half of the connections are excitatory and half inhibitory.

The firing rate of neuron i is r_i where $r_i = R_0 + \phi(x_i)$ with $\phi(x) = R_0 \tanh(x/R_0)$, $x \leq 0$, and $\phi(x) = (R_{max} - R_0) \tanh(x/(R_{max} - R_0))$, $x > 0$. R_0 is the background firing rate and R_{max} is the maximum rate. Averaging over all r_i, $i = 1$ to $\mathcal{N}$, then gives the average activity in the network.

An important part of the present investigation concerns the interaction between modules (subsets) of neurons. Each module is capable of sustained activity without any external input. The modules are then linked by connections with synaptic strength $g_{ext.}$ The number of connections can also be varied.

Model 2

This model uses a network of integrate-and-fire neurons. Figure 1 depicts a system of three interconnected modules, each containing an identical neural network. (The labels DLFPC, Parietal and Occipital are to indicate representative cortical regions, but no detailed modeling of different regions is undertaken.) Each module contains pools of excitatory neurons (red triangles) and inhibitory neurons (green circles), synaptically connected within and between pools (black arrows). The long red arrows indicated connections between the excitatory neurons in different modules; the strength of these connections can be modified, for example by input from a basal nucleus, indicated by green lines. The two outer modules can also be connected (not shown in the figure).

The formalism below is a simplified version of that of [36]; see also [37].

The membrane potential V of a single neuron is governed by

$$\frac{dV}{dt} = -g_L(V - V_L) - g_E(t)(V - V_E) - g_I(t)(V - V_I), \quad (2)$$

where g_L is the leak conductance, $g_E(t)$ and $g_I(t)$ are the time-dependent conductances arising from external inputs and from the network activity of excitatory and inhibitory neurons. These have been normalized by the membrane capacitance and thus have dimensions of inverse time. V_L is the rest potential and V_E, V_I are the excitatory and inhibitory reversal potentials.

The membrane potential of a neuron evolves according to integrate-and-fire dynamics. A spike is generated when $V = V_T$; V is then reset to $V_R (< V_T)$ and held there for an absolute refractory period τ_{ref}. The membrane potential is normalized so that $V_T = 1$ and $V_R = 0$.

We model a network of $\mathcal{N}$ neurons, of which N_E are excitatory and N_I are inhibitory. The conductance change in a typical neuron due to excitatory inputs is

$$g_E(t) = g_E^0(t) + \sum_k A_k \sum_l G_E(t - t_l^k), \quad (3)$$

where g_E^0 is the contribution from external excitatory sources, A_k is the connection strength from the kth excitatory neuron and $G_E(t - t_l^k)$ describes the effect of the post-synaptic current generated by an action potential in neuron k at time t_l^k. This function is taken to have an α-like form:

$$G_E(t) = \frac{1}{6\tau_E} \left(\frac{t}{\tau_E}\right)^3 \exp(-t/\tau_E) \, \theta(t), \quad (4)$$

where $\theta(t) = 1$ for $t > 0$ and 0 otherwise; τ_E is the time constant for

excitatory neurons. The sum $\sum_k$ is over all neurons connected to the excitatory neuron under consideration and $\sum_l$ is over all firings of neuron k up to time t. Similarly, the conductance change in a typical neuron due to inhibitory inputs is

$$g_I(t) = g_I^0(t) + \sum_k B_k \sum_l G_I(t - t_l^k), \quad (5)$$

where $G_I(t)$ is given by Eq 3 with τ_E replaced by τ_I. The connection strengths A_k and B_k generally have a dependence on the spatial separation of the neurons (usually taken to be a Gaussian) and also can depend on the excitatory or inhibitory nature of the coupled neurons, but in our simplified model we set $A_k = B_k = S$, where S is a constant. (Investigations using Gaussian spatial dependence indicate that this simplification does not significantly alter the results reported here.) The sums over k in Eqs 3 and 5 are over all neural connections; in the computations, a fraction F of all N neurons are connected, with no distinction made between excitatory and inhibitory neurons.

The time-evolution of the network is initiated by a random inputs (Poisson trains) applied separately to each neuron. Temporal updating uses a modified second-order Runge-Kutta scheme [38]. The external Poisson train is applied for 500 ms, then removed and the system allowed to evolve freely for a further 500 ms, during which time it reaches a steady state in which the average firing rate remains constant; data is then collected over the next 500 ms. (Some typical firing trains are shown in Figure S1.).

Again, we investigate the interaction between modules (subsets) of neurons (Figure 1). The connections between the modules may be only excitatory or both excitatory and inhibitory as they give very similar results. The parameter S_{ext} gives the connection strength and F_{ext} gives the fraction of connections between neurons in different modules.

Parameter Choice

The crucial requirement is that the network in an isolated module settles into a stable state that is neither dead (zero firings) nor one in which all neurons are firing at their maximum rate. This requirement places quite severe restrictions on the range of parameter values that can be used. For both models we did extensive tests varying the number of neurons and the strengths and number of synaptic connections. For Model 1 it was found that 1000 neurons were sufficient to give consistent results. The main other adjustable parameter is the synaptic strength g, and this was varied in the range $1 < g < 2.5$. For larger values the firing rates became oscillatory, rather than steady. We note that [33] used $g = 1.5$ as a typical value. For Model 2 various sized networks were investigated, ranging from 900 to 10,000 neurons. In each case, a connection fraction F was first chosen and then the synaptic strength S was adjusted to obtain a stable state. For example, the choice $\mathcal{N} = 900$, $F = 0.2$ and $S = 0.0085$ gave a stable state with a firing rate of about 85 Hz. For $\mathcal{N} = 10,000$ and $F = 0.2$, S had to be adjusted to 0.00075 to give a similar result; for some results involving networks of different sized, see Figure S2B. (A firing rate of 85 Hz is of course much higher than experimentally observed, but this is a consequence of the necessity of using model networks with many fewer neurons than physiological ones; see, for example, [39]. Most calculations were done using networks with more than 2000 neurons, as the averaging over spike trains gave more consistent results. The number of excitatory neurons was fixed at 80% of the total for the calculations reported here, but varying this did not significantly change the results. For calculations involving 2 or 3 modules, each module is an identical network, with parameters chosen to give stable states when the

Table 1. Parameter values in the Models.

Quantity	Symbol	Value	Notes
Model 1			
Number of neurons	N	1000	
Membrane time constant	τ	10 ms	[35]
Intra-modular synaptic strength	g	various	
Inter-modular synaptic strength	g_{ext}	various	
Background firing rate	R_0	0.1	[35]
Maximum firing rate	R_{max}	1.0	[35]
Model 2			
Number of excitatory neurons	N_E	various	
Number of inhibitory neurons	N_I	various	
Rest potential	V_L	0	[37]
Excitatory reversal potential	V_E	14/3	[37]
Inhibitory reversal potential	V_I	$-2/3$	[37]
Absolute refractory period	τ_{ref}	5 ms	
Leak conductance	g_L	0.05 ms^{-1}	[37]
Excitatory decay time	τ_E	1 ms	adjusted
Inhibitory decay time	τ_I	5/3 ms	adjusted
Intra-modular neuronal coupling strength	S	various	
Inter-modular neuronal coupling strength strength	S_{ext}	various	
Intra-modular connection fraction	F	various	
Inter-modular connection fraction	F_{ext}	various	

doi:10.1371/journal.pone.0060518.t001

modules are uncoupled. Then either the inter-modular neuronal coupling strength S_{ext} or the inter-modular connection fraction F_{ext} is varied. Tests were also performed where the inter-modular connections were purely excitatory, but differences were not significant. Parameter values used in the calculations are listed in Table 1.

Results

Theoretical: Predicted Changes in the Functioning of Cortical Areas on Changing the Extent of their Inputs

This theoretical section is necessary to answer the following specific questions in the Results: Is about half of the activity in a particular area of cortex dependent on its associational synaptic connections with other areas of cortex? Is the observed decline in associational connections in schizophrenia sufficient to account for the observed decline in activity in the areas of cortex subserved by these connections?

Computational estimates (Model 1). Figure 2 shows the computational solutions for different values of g (the strength of intra-modular synaptic connections) in the case of two coupled cortical modules. This indicates that for decreasing inter-modular synaptic strength g_{ext} there is an increase in the extent of decline in activity within the modules (Figure 2). This is such that a 24% decrease in inter-modular synaptic coupling strength leads to a decrease in activity of 6.5%, 8.5% and 10% for g values of 2.5, 2.0 and 1.5 respectively. As is shown below, if cortical activity is measured in schizophrenia it declines by similar percentages (4% to 7%) when there is a 24% decrease in the integrity of longitudinal fascicles supplying the synaptic coupling between

different cortical areas, identified here as different modules. If, for $g = 1.5$, the inter-modular synaptic coupling strength is reduced to zero, then the activity within the modules is reduced by 47%, which, as shown below, is about the reduction in activity of cortical areas observed when they are deprived of any coupling. Calculations were also performed in which the number of inter-modular synaptic connections was reduced. The results differ by less than a maximum of 10% from those in Figure 2.

Simulation estimates (Model 2). The extent of modular activity as measured using network activity with changes in the extent of synaptic coupling between modules (Figure 1) has been determined in simulations. These show that there is very little change in the curves relating network activity to the extent of synaptic coupling between modules (Figure 3A) for the three module case given in Figure 1. In the example shown for illustration, the intra-modular synaptic coupling fraction is fixed at $F = 0.3$.and initially the inter-modular coupling fraction F_{ext} is given the same value; that is each neuron is on average connected to 0.3 of all the intra- and inter-modular neurons. Decreasing the number of inter-modular synaptic couplings by 24% decreases network activity by about 7%, and decreasing these couplings to zero decreases network activity by about 50% (Figure 3A). These values are similar to those for the computational solution (Figure 2) and so are similar to the observations in schizophrenia as noted above and indicated in detail below. Additional computations were performed for different sized networks and connection fractions. It was found that provided the initial connection fractions were the same $(F_{ext} = F)$ then the decrease in network activity as F_{ext} is reduced is similar to that shown in Figure 3A. (Some additional results are given in Figure S2.).

It should be noted that there is an equivalence between the extent of decrease in modular activity and the fraction of inter-modular synaptic connections on the one hand with the decrease in modular activity and the strength of the inter-modular synaptic connections on the other (Figure 3B). So either a loss of inter-modular synaptic connections or a decrease in the efficacy of
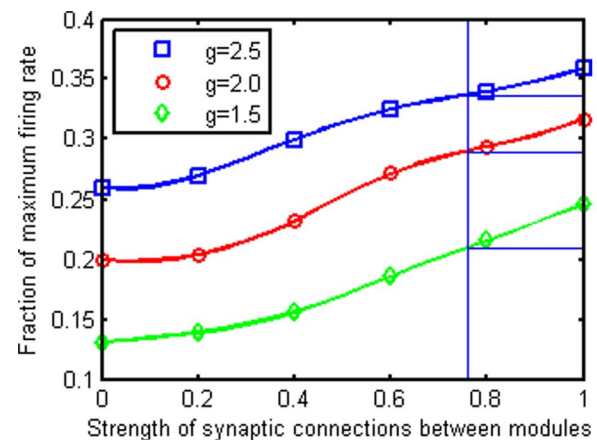

Figure 2. Firing rates for a two-module network. The simulation uses Model 1, with parameter values given in Table 1; each module contains 1000 neurons. The firing rate, normalized by the maximum firing rate, is plotted against the strength g_{ext} of synaptic connections between the two modules for three values of the intra-modular synaptic strength parameter g. The overall decreases in firing rate as the inter-module connection decreases from fully coupled to completely uncoupled are 47%, 37% and 28% for $g = 1.5$, 2.0 and 2.5, respectively. The corresponding decreases as the connection strength decreases by 24% (vertical line) are 10%, 8.5% and 6.5%, respectively.
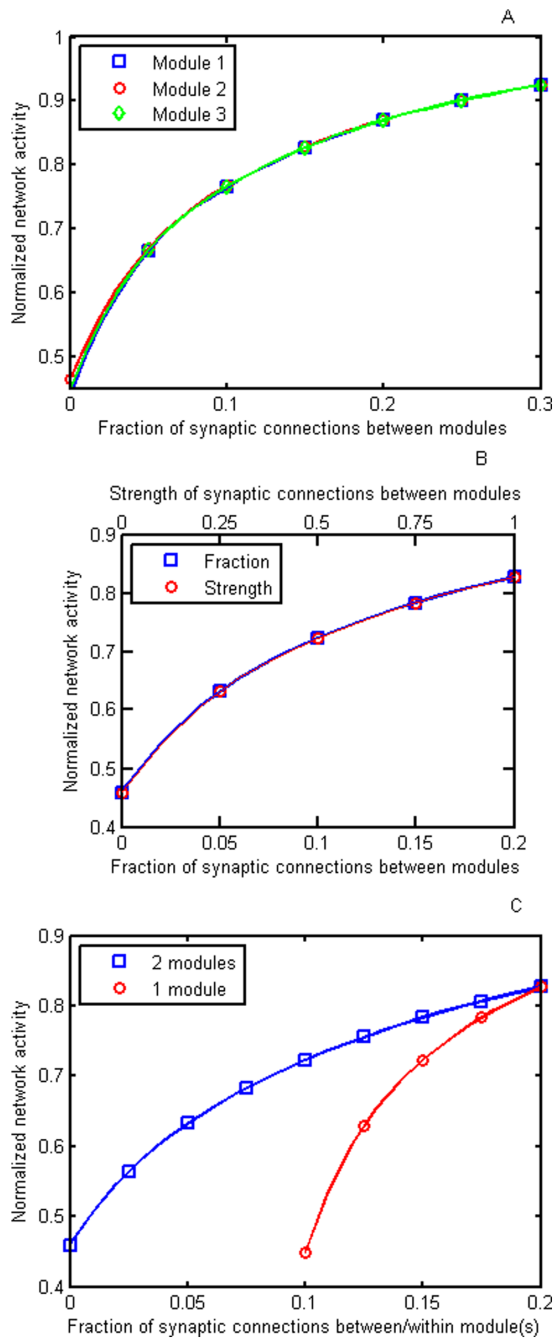doi:10.1371/journal.pone.0060518.g002

Figure 3. Results for the simulations of Model 2 giving changes in the activity in the modules (normalized by the maximum activity) with changes in inter-modular synaptic connections. A, comparison between activity and decreases in the fraction of inter-modular synaptic connections (F_{ext}) for three modules (results for each of the three modules indicated by open squares, open circles and open triangles, respectively). Note that there is very little difference in the changes in the normalized activity with changes in the inter-modular extent of synaptic connections for any of the modules. The intra-modular synaptic connectivity fraction F was kept at 0.30 for each module and the coupling strength is $S = 0.00075$. The number of neurons in each module was 3267 (99×33). B, comparison between normalized activity in the modules and decreases in the fraction of inter-modular synaptic connections (F_{ext}) between them on the one hand (open squares) and activity in the modules and decreases in the strength of synaptic connections on the other (open circles). This is a two modular case, with the results for just one module shown as the

other one had identical activity; similar results were obtained for the three module case. The intra-modular synaptic connectivity F was kept at 0.2 and the coupling strength is $S = 0.0015$. The number of neurons in each module was 2450 (70×35). Note that for the values given in the abscissa there is no difference between changing the extent of inter-modular synaptic connections and changing the strength of the connections. C, comparison between normalized activity in the modules and decreases in the fraction of inter-modular synaptic connections (F_{ext}) between them for the case when the intra-modular extent of synaptic connections was kept at 0.20 (open squares) and the case in which the extent of both inter-modular and intra-modular synaptic connectivity was reduced to the same extent (open circles); $S = 0.0015$ The number of neurons in each module was 2450 (70×35).
doi:10.1371/journal.pone.0060518.g003

synapses subserving these connections or a combination of both will retain the relation between modular activity and modular connectiveness.

Simulations allow a comparison to be made between the extent of decrease in network activity following a decrease in the inter-modular synaptic connections on the one hand and the decrease in network activity following a decrease in both inter-modular and intra-modular synaptic connections on the other. It is only necessary to decrease all the synaptic connections by half in order, in the example shown in Figure 3C, to halve network activity whereas, as previously shown (Figure 3A), if only inter-modular synaptic connections change then these must be reduced to zero in order to reduce network activity by 50%.

Experimental: Observed Changes in the Functioning of Cortical Areas on Changing the Extent of their Inputs

CMRglc(ox) required to sustain local cortical networks in isolated cortical areas. Isolated slices of cortex possesses a $CMR_{glc(ox)}$ in rats of 0.51 ± 0.05 μmol/g/min, compared with the normal $CMR_{glc(ox)}$ of 1.01 ± 0.03 μmol/g/min (Table S1), so there is a 49% decrease in $CMR_{glc(ox)}$ (Figure 4). Thus the ongoing activity of the cortex remains high even in the absence of thalamic, forebrain and associational fiber connections. This decrease in $CMR_{glc(ox)}$ of about 50% when the cortical area under consideration is deprived of its inputs is about the same as that predicted by both the computational (Figure 2) and simulation models (Figure 3) when the inter-modular synaptic connections are reduced to zero, given that $CMR_{glc(ox)}$ is proportional to network electrical activity [31].

CMRglc(ox) required to sustain local cortical networks deprived of their long associational-fiber connections. Another test of the model is to consider the $CMR_{glc(ox)}$ decrease in a local cortical area consequent on reducing most of the inputs into the area by removing major associational-fiber inputs. A cold lesion applied to the surface of the rat parietal cortex transiently blocks all activity in the underlying white matter including longitudinal association fibers [40]. The longitudinal fibers from parietal cortex are the most extensive in the brain. Medial and dorsal parietal lobe projects through superior longitudinal fasciculus components I, II and III as well as the fronto-occipital fasciculus and middle longitudinal fasciculus [5]. Lesion of these will disturb $CMR_{glc(ox)}$ in the frontal and prefrontal, premotor/supplementary motor area and occipital cortex [5]. This is reflected in the measured $CMR_{glc(ox)}$ changes following cold lesion of the parietal cortex, with decreases of $47 \pm 5\%$ in frontal cortex (Table S2; from 1.0 ± 0.03 to 0.53 ± 0.05 μmol/g/min; [40,41]), $51 \pm 8\%$ in sensorimotor cortex (Table S2; from 1.07 ± 0.04 to 0.52 ± 0.05 μmol/g/min; [40,41]) and in one measurement, 55% in the occipital cortex (Table S2; from 0.94 ± 0.03 to 0.42 ± 0.03 μmol/g/min; [40–42]). The

average decrease in $CMR_{glc(ox)}$ across the cortex is $49.2\pm2.5\%$ (Table S2). Given that the parietal white matter lesions lead to the loss of a substantial part of the input to the named cortical areas then the 49% decrease in $CMR_{glc(ox)}$ in these areas is in accord with the computational and simulation modeling (Figures 2 and 3).

$CMRglc(ox)$ expenditure in cortical areas deprived of their brain-stem basal forebrain/intralaminar thalamic inputs. The excitability of a particular cortical area is also determined by the brain-stem basal forebrain and the intra-laminar thalamic inputs, besides the longitudinal associational inputs already considered. Although the cold lesions to the parietal cortex considered above may not substantially interfere with inputs from the basal forebrain and thalamus to cortical areas other than parietal, it is of considerable interest to determine this forebrain and thalamic contribution to cortical $CMR_{glc(ox)}$.

Lesions to the nucleus basilis magnocellularis (NBM) in rodents, the homologue of Meynert nucleus in primates, gives $29\pm1\%$ decrease in $CMR_{glc(ox)}$ (Table S2 and Figure. 4; [43]). A lesion to the Meynert nucleus in primates reduces the normal $CMR_{glc(ox)}$ by $37\pm9\%$ in prefrontal, parietal, occipital and temporal cortex [44,45]; (Table S4). There is then very substantial loss of $CMR_{glc(ox)}$ upon lesioning these nuclei.

$CMR_{glc(ox)}$ measurements following lesioning of the intra-laminar thalamic input to the primate and rodent cortex from the centromedian, parafascicular, central lateral and midline nuclei have been made [46]. Lesioning of the thalamus gives rise to a widespread decrease of $CMR_{glc(ox)}$ throughout the cortex, which is less than one third of that following lesioning of NBM or the nucleus of Meynert (see Tables S2(rat) and S4 (human); [47,48]). These quantitative estimates of $CMR_{glc(ox)}$ indicate that

the basal forebrain nuclei play the dominant role. Simply adding forebrain and thalamic contributions to the $CMR_{glc(ox)}$ suggests that about half of all cortical excitability, 54% in primates and 41% in rats, is dependent on these inputs (Figure 4).

The result of the calculation and modeling is that transient cold block lesioning of the parietal cortex, interrupting the main longitudinal associational projections between this parietal cortex and a number of other areas, gives rise to very substantial decreases in $CMR_{glc(ox)}$, of about 50%, within frontal, occipital and sensorimotor area. It might be argued that the decrease of about 50% within frontal, occipital and sensorimotor areas on cold lesioning of the parietal cortex is not only due to interrupting the main long associational projections but is also due to interruption of the basal forebrain projections to these regions However for this to occur there would have to be very substantial retrograde loss of their projections for there is a rostro-caudal innervation of the cortex by the basal forebrain nuclei, with the frontal regions innervated well before the parietal [49]. Furthermore, the innervation of the hippocampus by the basal forebrain nuclei in the rat occurs well caudal to the basal forebrain nuclei [50], yet no significant changes in $CMR_{glc(ox)}$ have been reported for the hippocampus following parietal lesions. It is suggested here that interruption of the parietal longitudinal associational fibers, the SLF, is primarily responsible for the loss of about 50% $CMR_{glc(ox)}$ in the frontal regions, as well as in the sensorimotor area.

$CMRglc(ox)$ expenditure required to sustain intrinsically determined as well as extrinsically determined excitability of local cortical networks. It is evident from Figure 4 that addition of the different sources of cortical excitability, measured using $CMR_{glc(ox)}$, whether intrinsic, dependent on longitudinal
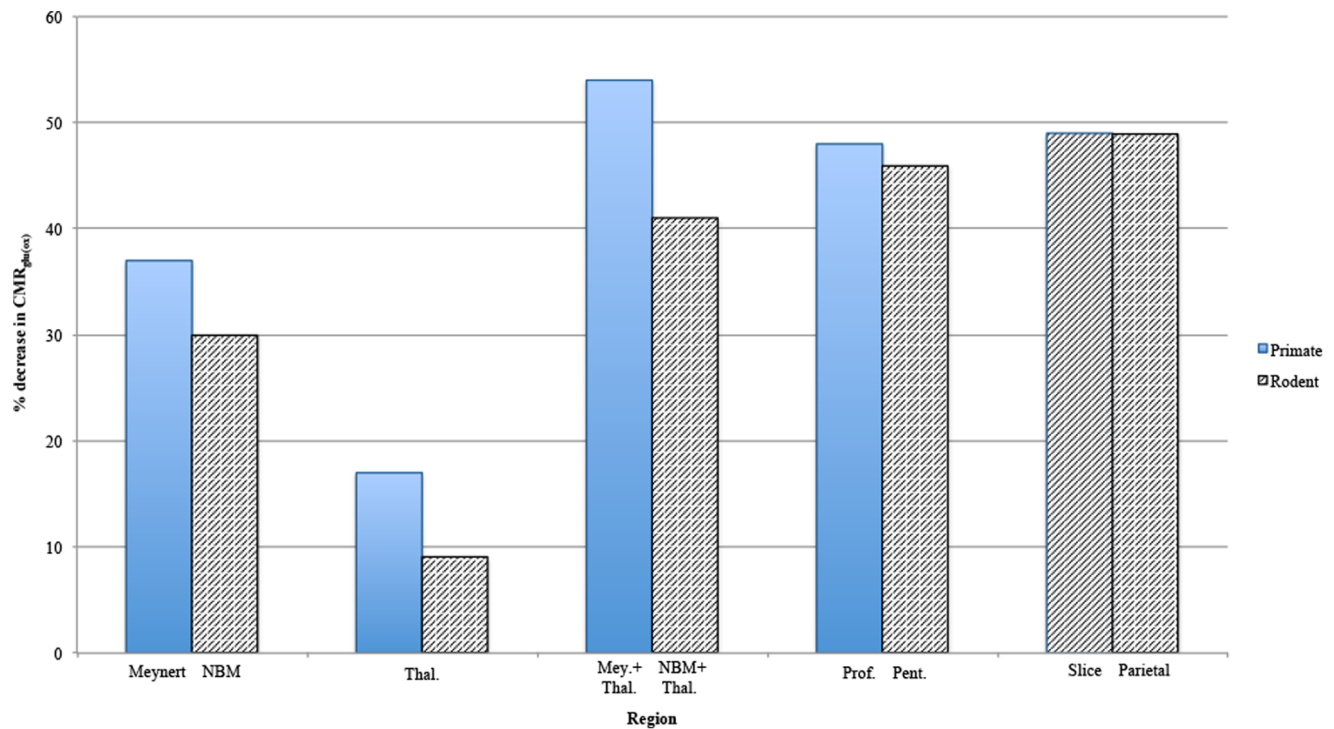

Figure 4. Histogram of the average percentage decreases in $CMR_{glc(ox)}$ determined in rat and primate brains under the experimental conditions given in the abscissa. $CMR_{glc(ox)}$ is proportional to network activity (Hyder *et al.,*2013). For primate (blue bars) these are from left to right: lesion of the nucleus of Meynert; the thalamic intralaminar nuclei (Thal); the nucleus of Meynert plus the thalamic nuclei (Mey+Thal); and under the anaesthetic propofol (Prof). For the rat (grey bars) these are from left to right: lesion of the nucleus basilis magnocellularis (NBM); the thalamic intralaminar nuclei (Thal); the NBM plus the thalamic nuclei (NBM+Thal); under the anaesthetic pentobarbital (pent); slices of cortex (slice); and lesion of the parietal cortex (Parietal). The percentages given in this histogram are from Tables S2 to S5.
doi:10.1371/journal.pone.0060518.g004

associational fibers or on brain-stem basal forebrain/intralaminar thalamic inputs, adds up to about 150% of the normal awake $CMR_{glc(ox)}$. Clearly one or more of these sources of excitability must be dependent on the other. Thus removal of the diffuse cholinergic innervation of the cortex by the brain stem nuclei leads to a 30% to 37% decrease of $CMR_{glc(ox)}$ in rats and primates (Figure 4). If this is added to the decrease on lesioning the thalamus of 9% to 17% for rats and primates (Figure 4) then about half of the $CMR_{glc(ox)}$ utilization in the cortex is dependent on these activating nuclei (Figure 4). This agrees with the known changes in $CMR_{glc(ox)}$ during slow wave sleep in humans (38%, Table S3; [51] when the brain-stem excitability systems that project to the basal-forebrain nuclei and the non-specific nuclei of the thalamus are largely inactive. If this is the case then it might be argued that the diffuse cholinergic nuclei are necessary for the functioning of the networks composed by these associational fibers, with the major energy expenditure occurring as a consequence of the activity in the network not in energy expenditure required to sustain the direct input from the diffuse cholinergic nuclei. According to this scenario, these nuclei then trigger the activity in the associational-fiber networks, and this triggering does not consume much energy (Figure 1). If this is the case then about 50% of $CMR_{glc(ox)}$ is expended in maintaining the local networks and 50% $CMR_{glc(ox)}$ to maintaining the associational networks.

Schizophrenia: Predicted and Observed Changes in the Functioning of Cortical Areas and their Inputs

Here we compare the changes in $CMR_{glc(ox)}$ in the cortex of schizophrenia patients and the predictions of the model (Figure 1) following DTI determination of deterioration of their SLF.

The superior longitudinal fasciculus in schizophrenia: white matter deterioration measured with DTI. Fractional anisotropy decreases of 24.6±4.1% are measured in the SLF in schizophrenia (Table S5).

Cortical function in schizophrenia: decreases in CMRglc(ox) in cortical areas. Fourteen studies have noted changes in $CMR_{glc(ox)}$ in different cortical areas of schizophrenia patients and seven studies measuring changes in regional cerebral blood flow (rCBF) in such patients (Table S6). The observations indicate percentage decreases in the cortex of 6% to 5% in frontal regions, 7% in temporal regions, and a lesser amount of 4% in parietal regions (Table S6). The predicted decrease from the model of Figure 1, as the graph in Figure 3B shows, is 6% for a 25% decrease in connectivity as measured with DTI. There is then good agreement between the predicted and observed decreases in cortical function following deterioration of the longitudinal fasciculus.

It will be noted in Table S6 that there is a 7% decrease in $CMR_{glc(ox)}$ in the thalamus. As lesioning the intralaminar nuclei of the thalamus only gives rise to a 17% decrease in $CMR_{glc(ox)}$ in the primate cortex (Figure 4), a 7% decrease in thalamic function is unlikely to contribute significantly to the decrease in cortical $CMR_{glc(ox)}$. There are no measurements of $CMR_{glc(ox)}$ in the basal nucleus of Meynert available in patients with schizophrenia; however recent observations suggest that the cholinergic pathways that mediate the projection of the nucleus of Meynert to the cortex are little compromised in schizophrenia [52].

Another consideration should be mentioned here and that is whether changes in intracortical synaptic connections are likely in schizophrenia, independent of changes in synaptic connections subserving the principal inter-cortical connections, like the superior longitudinal fasciculus. According to Figure 3C if both intercortical and intracortical connections are lost in schizophrenia there will be a much greater decrease in $CMR_{glc(ox)}$ than when just

the former are lost. Using fMRI and graph theory it has been claimed that there is a loss of intracortical connections in schizophrenia. If such a loss produces significant decreases over and above that due to the loss of intercortical connections then the present predictions will have to be modified.

Discussion

Modeling the Cortex in the Context of Schizophrenia: Cortico-cortical Synaptic Connections

The principal evidence in favor of the present model of the role of associational fibers in cortical function (Figure 1) is that changes in $CMR_{glc(ox)}$ on removing associational connections, either by transient cold blocks or by lesions as in slices, is that predicted, given that electrical network activity is proportional to $CMR_{glc(ox)}$ [31] (see Figures 3 and 4). However there are two caveats concerning the interpretation of the changes in the $CMR_{glc(ox)}$ throughout the cortex following cold block of the rat parietal cortex (Table S2). One of these is that the distribution of fiber pathways has been determined for primate brain, using both autoradiography and DTI, to a high degree of accuracy [53,54], whereas those for the rat brain have only recently become available [55,56]. These show that there are reasonable homologies with respect to these pathways between the species: see for example the projection of the medial longitudinal fasciculus [57]; the cingulum bundle [58]; and the arcuate fasciculus [59,60]. The identification of the fiber pathways interrupted in the experiments using transient cold block placed over the rat parietal cortex is to some extent dependent on these homologies so that the $CMR_{glc(ox)}$ results in Table S2 must be considered with this reservation. Another reservation concerning Table S2 is that the values of $CMR_{glc(ox)}$ used to determine the percentage decreases are the maximum observed and not those during the substantial recovery that often occurs over time in $CMR_{glc(ox)}$.

Some mention should be made of the sources of experimental data, shown in the Tables (Supplement) and mostly summarized in Figure 4, which were used to test the models. The $CMR_{glc(ox)}$ data presented in Tables S1, S2, S3, S4, S5 and S6 are all from in vivo experiments, with only that for rodent cortical slices in Table S1 being of necessity from in vitro experiments. Thus all the histogram bars in Figure 4, with the exception of the second last one (reading from left to right) are from in vitro measurements. The two species considered are rats and baboons and these are presented for comparison, as the changes in $CMR_{glc(ox)}$ in the different experimental conditions are qualitatively very similar for both species (see Figure 4). The one comparison between in vivo and in vitro conditions is for the cortical slice versus the intact isolated parietal cortex (last two histogram bars in Figure 4) and it is of interest that these give the same changes in $CMR_{glc(ox)}$.

Diffusion tensor imaging has noted decreases in fractional anisotropy changes in the uncinate fasciculus, joining the temporal lobe adjacent to the amygdala and the ventrolateral prefrontal cortex/orbitofrontal cortex, associated with emotional experiences, in schizophrenia [61], in addition to the changes noted above (Table S5) in the SLF (for a review of these pathways, see [19]). The measure of diffusivity in this imaging can be determined in three directions through a fiber tract, lambda I associated with the integrity of axons and lambdas II and III with that of myelin [62–65]. Changes in lambda II and lambda I predict the evolution in multiple sclerosis of severe tissue damage, including axonal swelling and loss of axons in a tract [66]. The full power of this approach has not yet been used on the principal fasciculi of the cortex in schizophrenia. It is interesting to note that changes in

anisotropy of fasciculi in cognitive impairment is associated with a loss of gray matter in the cortical areas these fasciculi join [67].

Modeling the Cortex in the Context of Schizophrenia: Subcortical-cortical Synaptic Connections

$CMR_{glc(ox)}$ almost doubles in the awake state from deep sleep, and changes in $CMR_{glc(ox)}$ on removing associational connections in the awake animal are about those found in slices. This suggests that the activating system, comprising thalamic and basal nuclei, operates without much expenditure of energy to trigger functioning of the associational connections that are responsible for the differences between the awake and deep-sleep states. The model considered here for probing the role of associational fibers in cortical function (Figure 1) has been primarily tested by considering changes in $CMR_{glc(ox)}$ following lesions to the cortex that interrupt these fibers. However, is the model consistent with changes in $CMR_{glc(ox)}$ observed during sleep? This is now considered.

The primary form of brain damage in closed head injuries (Xu et al., 2007) leading to a posttraumatic persistent vegetative state appear to be focal axonal injuries in the dorsolateral brain stem, including the ascending reticular activation [68]. Damage to the brain stem tegmentum, bilaterally, either in the pons alone or in the upper pons and midbrain, leads to coma whereas damage to the brain stem outside the tegmentum does not [69,70]. Reversible inactivation of the brain-stem nuclei leads to an anesthesia-like state or coma [71]. It is therefore clear that the integrity of brain-stem structures is essential for maintaining consciousness. The meso-pontine tegmental area of the brain stem projects to (i) intralaminar thalamic nuclei that in turn project over the cortex; (ii) to several pontomesencephalic, diencephalic and basal forebrain nuclei that also project to cortex, as well as to areas in the (iii) subcortical forebrain such as the hypothalamus, the septal area, the zona incerta and striato-pallidal system with some (iv) direct projections to the frontal cortex [72]. The ascending brain stem arousal system modulates the thalamo-cortical system, principally via the intra-laminar thalamic nuclei, and has often been considered to be a major source of neocortical electrical activity as measured by the electroencephalogram during cortical arousal in wakefulness [73–75]. The ascending brain stem arousal system projection to basal forebrain neurons gives rise to activity in the neurons that correlates with wake-sleep patterns and electroencephalographic waveforms [2,76], with some suggesting that these basal nuclei play a more diffuse role in cortical arousal than that provided by the thalamic nuclei [77]. However lesions or local inactivation of the thalamic nuclei with lidocaine does not antagonize persistent cortical activation [78–81]. On the other hand injections of the local anesthetic procaine into the basal forebrain does [82] as do lesions of this nucleus [83,84]. Recently it has been shown that extensive thalamic lesions have little effect on electroencephalographic or behavoural measures of wakefulness whereas animals with large basal forebrain lesions or lesions to the brain stem parabrachial-precoeruleus are behaviourally unresponsive and possess a monot-onous sub-1 Hz electroencephalogram during continuous gentle handling [85]. Lesions to the nucleus basalis of Meynert (baboon) or the nucleus basilis magnocellularis (rat) removes substantial cholinergic innervation of the principal lobes of the cortex, including prefrontal, parietal, temporal, occipital and cingulate cortex [49]. Lesions to the remaining basal forebrain nuclei (in the rat; the diagonal band of Broca and the medial septal nuclei) removes cholinergic innervation from the hippocampus (including subiculum and entorhinal cortex) and medial mesolimbic cortex and part of the occipital cortex [50], so that it appears that these nuclei play a principal role in maintaining cortical excitability at a level sufficient for consciousness.

Alterations between being awake and sleep are determined by groups of neurons in the ascending reticular activating systems, which activate cholinergic neurons in the basal forebrain that fire during waking but markedly decrease their firing during slow-wave sleep in contrast to GABAergic neurons (principally in the basal forebrain that act in the opposite way [86]. In the prefrontal cortex layer 3 pyramidal neurons are the principal origins of cortico-cortical connections, including those of the SLF [87]. The primary effect of the acetylcholine released from the NBMin rodents and the nucleus of Meynert in primates is to act on m_2 muscarinic receptors found on synaptic spines, where they facilitate synaptic transmission in the long projection fiber tracts (for a recent summary of these facilitatory mechanisms, see [88]. The projection of these nuclei to the cortex may be regarded as serving the role of supplying a tuneable effect that controls the efficacy of inter-modular connections. This amounts to changing the parameters g_{ext} (Model 1) or S_{ext} and/or F_{ext} (Model 2). In visual cortex at least 50% of neurons in layer 2/3 possess these muscarinic receptors (Figure 2 in [88], which overwhelmingly produces a facilitating effect on glutamatergic transmission to these neurons [88]; see their Figure. 8B) The m_1 and m_2 receptors are on spines that are contacted by noncholinergic afferents [89–92] so that transmission from cholinergic afferents is very likely to involve the diffusion of acetylcholine from the terminals over relatively long distances as in volume transmission, as described by Fuxe and colleagues [93] and as occurs prominently in the peripheral autonomic nervous system [94]. Such transmission involves activation of G-proteins that give rise to effects that typically operate in the seconds time domain [95]. Of particular interest is that these facilitatory effects due to acetylcholine are maintained for over an hour after cessation of the action of acetylcholine on muscarinic receptors [96,97], perhaps indicating very little energy expenditure to maintain the facilitatory state after the acetylcholine has ceased to be released.

Transcranial magnetic stimulation (TMS) of the cortex during slow wave sleep reveals, as in the case of anaesthetics, that activation only occurs at the site/area stimulated [98], with the subject declaring no recollection of any consciousness during the period [99]. However in rapid eye movement sleep, when subjects are unresponsive to sensory stimuli but rather have dreams which they report on when awake, the cortical response to TMS again shows sequential activation throughout the cortex [100], as in the awake state. These observations suggest that the longitudinal associational connections are not active in slow-wave sleep as they are when awake, and confirm the present hypothesis concerning the functioning of the brain-stem basal forebrain/intralaminar thalamic cortical network.

Implications of the Cortical Model in Schizophrenia

The model that emerges from this work is that about 50% of $CMR_{glc(ox)}$ is required to sustain spontaneous activity of different cohorts of neurons in local networks representing different aspects of a cortical areas functions, such as orientation in V1. Input from the thalamus triggers sets of these cohorts through a relatively low $CMR_{glc(ox)}$ consumption mechanism. The remaining 50% of $CMR_{glc(ox)}$ is primarily required to sustain spontaneous activity in the associational networks representing global aspects of the functions of cortical areas, such as those involving V1 and MST in the visual system. The triggering of these associational networks by basal forebrain nuclei and from the intralaminar nuclei of the thalamus also consumes very little $CMR_{glc(ox)}$ consumption.

In summary, a cortical model has been developed that quantitatively conforms with levels of electrical activity, measured using $CMR_{glc(ox)}$, under different experimental conditions. These

include the extent of changes in activity in cortex when isolated from all longitudinal and subcortical synaptic connections, when just longitudinal synaptic connections are removed and when subcortical synaptic connections are removed. The model quantitatively predicts the extent of decrease in activity observed in the cortex following the observed changes in function of longitudinal tract integrity but predicts a much greater change in cortical activity if significant changes in synaptic connections occur throughout the cortex (Figure 3C). This work points to the longitudinal associational fascicules as a major area of investigation in schizophrenia, a point emphasized in a recent review [101], for their deterioration explains both the observed changes in gray matter activity as well as the loss of synapses in the gray matter due to loss of associational synaptic connections.

Supporting Information

Figure S1 **Spike trains for three neurons in a Model 2 network.** In the first 500 ms the neurons are being driven by a random Poisson input which is then removed and the neurons settle into a stable firing pattern.
(TIF)

Figure S2 **Results for simulations of Model 2 for the case of two identical modules, showing changes in the network activity in one module with changes in inter-modular synaptic connections.** A. Decreases in network activity as the fraction of inter-modular connections (F_{ext}) is reduced, for 3 values of the intra-modular connection fraction, F. Each module contains 2450 neurons; the value $S = 0.0015$ is appropriate for this size of network and for the connection fraction $F = 0.2$. It is seen that starting with an inter-modular connection fraction $F_{ext} = F = 0.2$ (blue squares) gives the desired decrease, whereas starting with $F_{ext} = 0.25$ (red circles) or $F_{ext} = 0.15$ (green diamonds) gives decreases that are either too small or too large. B. Decreases in network activity as the fraction of inter-modular connections (F_{ext}) is reduced, for 4 different sized networks; N is the total number of neurons and each module contains half this number. The intra-modular connection fraction is $F = 0.2$ for all cases, and the appropriate S values are shown for each size of network. It is seen that the results converge as the network size increases.
(TIF)

Table S1 Experimental results for average $CMR_{glc(ox)}$ determinations (μmol/g/min) for the cortex of rodents in the conditions indicated [41–43,102–123].
(DOCX)

Table S2 Rodent changes in $CMR_{glc(ox)}$ following lesions. Changes in $CMR_{glc(ox)}$ in (μmol/g/min) in the cortical regions listed in the first column following lesions to the structures named in the first row. In each case the upper $CMR_{glc(ox)}$ is the control value and the lower $CMR_{glc(ox)}$ that following the lesion. The percentage change in each case is given in parenthesis [40,42,43,47,124]. **Key to first row**: NBM, nucleus basilis magnocellularis; Thalam, thalamus; Pariet, parietal cortex.
(DOCX)

Table S3 Experimental results for average $CMR_{glc(ox)}$ determinations (μmol/g/min) for the cortex of humans in the conditions indicated [51,125–138].
(DOCX)

Table S4 Primate changes in $CMR_{glc(ox)}$ following lesions. Changes in $CMR_{glc(ox)}$ (μmol/g/min) in the cortical regions listed in the first column following lesions to the structures named in the first row. In each case the upper $CMR_{glc(ox)}$ is the control value and the lower $CMR_{glc(ox)}$ that following the lesion. The percentage decrease in each case is given in parenthesis [44,48]. **Key to first row**: Meyn, nucleus of Meynert; Rhinal, rhinal cortex; Thal, thalamus.
(DOCX)

Table S5 Fractional anisotropy decrease of the superior longitudinal fasciculus in schizophrenia [19,139–142].
(DOCX)

Table S6 Percentage changes in $CMG_{glc(ox)}$ (rows 1–14) and rCBF (rows 15–21) in schizophrenia [32,114,143–161]. Note: Two papers report increases rather than decreases in rCBF in prefrontal regions of schizophrenia patients ([162,163]), with [162] reporting no differences in a subsequent paper [161]. These have not been included in this Table.
(DOCX)

Author Contributions

Neurobiological input: MB. Computation and software design: LF. Mathematical input: WG. Conceived and designed the experiments: MB. Analyzed the data: MB LF WG. Contributed reagents/materials/analysis tools: LF WG. Wrote the paper: MB WG.

References

1. Goldman-Rakic PS (1994) Working memory dysfunction in schizophrenia. J Neuropsychiatry Clin Neurosci 6: 348–357.
2. Lee MG, Hassani OK, Alonso A, Jones BE (2005) Cholinergic basal forebrain neurons burst with theta during waking and paradoxical sleep. J Neurosci 25: 4365–4369.
3. Silver H, Feldman P, Bilker W, Gur RC (2003) Working memory deficit as a core neuropsychological dysfunction in schizophrenia. Am J Psychiatry 160: 1809–1816.
4. Petrides M, Pandya DN (2002) Comparative cytoarchitectonic analysis of the human and the macaque ventrolateral prefrontal cortex and corticocortical connection patterns in the monkey. Eur J Neurosci 16: 291–310.
5. Schmahmann JD, Pandya DN, Wang R, Dai G, D'Arceuil HE, et al. (2007) Association fibre pathways of the brain: parallel observations from diffusion spectrum imaging and autoradiography. Brain 130: 630–653.
6. Chafee MV, Goldman-Rakic PS (1998) Matching patterns of activity in primate prefrontal area 8a and parietal area 7ip neurons during a spatial working memory task. J Neurophysiol 79: 2919–2940.
7. Chafee MV, Goldman-Rakic PS (2000) Inactivation of parietal and prefrontal cortex reveals interdependence of neural activity during memory-guided saccades. J Neurophysiol 83: 1550–1566.
8. Paulesu E, Frith CD, Frackowiak RS (1993) The neural correlates of the verbal component of working memory. Nature 362: 342–345.
9. Cole MW, Yarkoni T, Repovs G, Anticevic A, Braver TS (2012) Global connectivity of Prefrontal Cortex Predicts Cognitive Control and Intelligence. Journal of Neuroscience 32: 8988–8999.
10. Klingberg T (2006) Development of a superior frontal-intraparietal network for visuo-spatial working memory. Neuropsychologia 44: 2171–2177.
11. Narr KL, Bilder RM, Toga AW, Woods RP, Rex DE, et al. (2005) Mapping cortical thickness and gray matter concentration in first episode schizophrenia. Cereb Cortex 15: 708–719.
12. Whitford TJ, Grieve SM, Farrow TF, Gomes L, Brennan J, et al. (2006) Progressive grey matter atrophy over the first 2–3 years of illness in first-episode schizophrenia: a tensor-based morphometry study. Neuroimage 32: 511–519.
13. Minami T, Nobuhara K, Okugawa G, Takase K, Yoshida T, et al. (2003) Diffusion tensor magnetic resonance imaging of disruption of regional white matter in schizophrenia. Neuropsychobiology 47: 141–145.
14. Buchsbaum MS, Tang CY, Peled S, Gudbjartsson H, Lu D, et al. (1998) MRI white matter diffusion anisotropy and PET metabolic rate in schizophrenia. Neuroreport 9: 425–430.

15. Hao Y, Liu Z, Jiang T, Gong G, Liu H, et al. (2006) White matter integrity of the whole brain is disrupted in first-episode schizophrenia. Neuroreport 17: 23–26.

16. Kitamura H, Matsuzawa H, Shioiri T, Someya T, Kwee IL, et al. (2005) Diffusion tensor analysis in chronic schizophrenia. A preliminary study on a high-field (3.0T) system. Eur Arch Psychiatry Clin Neurosci 255: 313–318.

17. Kumra S, Ashtari M, McMeniman M, Vogel J, Augustin R, et al. (2004) Reduced frontal white matter integrity in early-onset schizophrenia: a preliminary study. Biol Psychiatry 55: 1138–1145.

18. Lim KO, Hedehus M, Moseley M, de Crespigny A, Sullivan EV, et al. (1999) Compromised white matter tract integrity in schizophrenia inferred from diffusion tensor imaging. Arch Gen Psychiatry 56: 367–374.

19. Karlsgodt KH, van Erp TG, Poldrack RA, Bearden CE, Nuechterlein KH, et al. (2008) Diffusion tensor imaging of the superior longitudinal fasciculus and working memory in recent-onset schizophrenia. Biol Psychiatry 63: 512–518.

20. Mesulam M-M (1995) Structure and Function of Cholinergic Pathways in the Cerebral Cortex, Limbic System, Basal Ganglia, and Thalamus of the Human Brain. In: Bloom F, Kupfer DJ, editors. Psychopharmacology– 4th Generation of Progress. New York: Raven Press.

21. Swenson R (2006) Review of Clinical and Functional Neuroscience. Dartmouth: Dartmouth Medical School.

22. Dierks T, Linden DE, Jandl M, Formisano E, Goebel R, et al. (1999) Activation of Heschl's gyrus during auditory hallucinations. Neuron 22: 615–621.

23. Kircher TT, Liddle PF, Brammer MJ, Williams SC, Murray RM, et al. (2001) Neural correlates of formal thought disorder in schizophrenia: preliminary findings from a functional magnetic resonance imaging study. Arch Gen Psychiatry 58: 769–774.

24. Shergill SS, Brammer MJ, Williams SC, Murray RM, McGuire PK (2000) Mapping auditory hallucinations in schizophrenia using functional magnetic resonance imaging. Arch Gen Psychiatry 57: 1033–1038.

25. Shergill SS, Bullmore E, Simmons A, Murray R, McGuire P (2000) Functional anatomy of auditory verbal imagery in schizophrenic patients with auditory hallucinations. Am J Psychiatry 157: 1691–1693.

26. Ford JM, Mathalon DH, Heinks T, Kalba S, Faustman WO, et al. (2001) Neurophysiological evidence of corollary discharge dysfunction in schizophrenia. Am J Psychiatry 158: 2069–2071.

27. Sigmundsson T, Suckling J, Maier M, Williams S, Bullmore E, et al. (2001) Structural abnormalities in frontal, temporal, and limbic regions and interconnecting white matter tracts in schizophrenic patients with prominent negative symptoms. Am J Psychiatry 158: 234–243.

28. Spence SA, Brooks DJ, Hirsch SR, Liddle PF, Meehan J, et al. (1997) A PET study of voluntary movement in schizophrenic patients experiencing passivity phenomena (delusions of alien control). Brain 120 (Pt 11): 1997–2011.

29. Shergill SS, Kanaan RA, Chitnis XA, O'Daly O, Jones DK, et al. (2007) A diffusion tensor imaging study of fasciculi in schizophrenia. Am J Psychiatry 164: 467–473.

30. Koch G, Ribolsi M, Mori F, Sacchetti L, Codeca C, et al. (2008) Connectivity between posterior parietal cortex and ipsilateral motor cortex is altered in schizophrenia. Biol Psychiatry 64: 815–819.

31. Hyder F, Rothman D, Bennett M (2013) Cortical energy demands of signaling and nonsignaling components in brain are conserved across mammalian species and activity levels. ProcNatlAcadSci USA 110: 3549–3554.

32. Yildiz A, Eryilmaz M, Gungor F, Erkilic M, Karayalcin B (2000) Regional cerebral blood flow in schizophrenia before and after neuroleptic medication. Nucl Med Commun 21: 1113–1118.

33. Abbott LC, Rajan K, Sompolinsky H (2011) Interactions between intrinsic and stimulus-evoked activity in recurrent neural networks. In: Ding D, Glanzman D, editors. The Dynamic Brain. Oxford: Oxford University Press.

34. Gerstner W, Kistler WM (2002) Spiking Neuron Models. Cambridge: Cambridge University Press.

35. Abbott LC, Rajan K, Sompolinsky H (2011) Interactions between intrinsic and stimulus-evoked activity in recurrent neural networks. In: Ding D, Glanzman D, editors. The Dynamic Brain. Oxford: Oxford University Press. 65–82.

36. Tao L, Shelley M, McLaughlin D, Shapley R (2004) An egalitarian network model for the emergence of simple and complex cells in visual cortex. Proc Natl Acad Sci U S A 101: 366–371.

37. Cai D, Rangan AV, McLaughlin DW (2005) Architectural and synaptic mechanisms underlying coherent spontaneous activity in V1. Proc Natl Acad Sci U S A 102: 5868–5873.

38. Shelley MJ, Tao L (2001) Efficient and accurate time-stepping schemes for integrate-and-fire neuronal networks. J Comput Neurosci 11: 111–119.

39. Amit DJ, Brunel N (1997) Dynamics of a recurrent network of spiking neurons before and following learning. Network: Comput Neural Syst 8: 373–404.

40. Pappius HM (1981) Local cerebral glucose utilization in thermally traumatized rat brain. Ann Neurol 9: 484–491.

41. Colle LM, Holmes LJ, Pappius HM (1986) Correlation between behavioral status and cerebral glucose utilization in rats following freezing lesion. Brain Res 397: 27–36.

42. Buczek M, Ratcheson RA, Lust WD, McHugh M, Pappius HM (1991) Effects of focal cortical freezing lesion on regional energy metabolism. J Cereb Blood Flow Metab 11: 845–851.

43. London ED, McKinney M, Dam M, Ellis A, Coyle JT (1984) Decreased cortical glucose utilization after ibotenate lesion of the rat ventromedial globus pallidus. J Cereb Blood Flow Metab 4: 381–390.

44. Kiyosawa M, Baron JC, Hamel E, Pappata S, Duverger D, et al. (1989) Time course of effects of unilateral lesions of the nucleus basalis of Meynert on glucose utilization by the cerebral cortex. Positron tomography in baboons. Brain 112 (Pt 2): 435–455.

45. Yamaguchi T, Kunimoto M, Pappata S, Chavoix C, Brouillet E, et al. (1990) Effects of unilateral lesion of the nucleus basalis of Meynert on brain glucose utilization in callosotomized baboons: a PET study. J Cereb Blood Flow Metab 10: 618–623.

46. Wiegell MR, Tuch DS, Larsson HB, Wedeen VJ (2003) Automatic segmentation of thalamic nuclei from diffusion tensor magnetic resonance imaging. Neuroimage 19: 391–401.

47. Raos VC, Dermon CR, Savaki HE (1995) Functional anatomy of the thalamic centrolateral nucleus as revealed by the [14C]deoxyglucose method following electrical stimulation and electrolytic lesion. Neuroscience 68: 299–313.

48. Szelies B, Herholz K, Pawlik G, Karbe H, Hebold I, et al. (1991) Widespread functional effects of discrete thalamic infarction. Arch Neurol 48: 178–182.

49. Selden NR, Gitelman DR, Salamon-Murayama N, Parrish TB, Mesulam MM (1998) Trajectories of cholinergic pathways within the cerebral hemispheres of the human brain. Brain 121 (Pt 12): 2249–2257.

50. Gaykema RP, Luiten PG, Nyakas C, Traber J (1990) Cortical projection patterns of the medial septum-diagonal band complex. J Comp Neurol 293: 103–124.

51. Buchsbaum MS, Gillin JC, Wu J, Hazlett E, Sicotte N, et al. (1989) Regional cerebral glucose metabolic rate in human sleep assessed by positron emission tomography. Life Sci 45: 1349–1356.

52. Rajii TK, Chow TW, Voineskos AN, Links KA, Miranda D, et al. (2012) Cholinergic pathways and cognition in patients with schizophrenia: A pilot study. Schizophrenia Research 139(1–3): 46–52.

53. Catani M, Thiebaut de Schotten M (2008) A diffusion tensor imaging tractography atlas for virtual in vivo dissections. Cortex 44: 1105–1132.

54. Schmahmann JD, Pandya DN (2007) The complex history of the fronto-occipital fasciculus. J Hist Neurosci 16: 362–377.

55. Johnson GA, Calabrese E, Badea A, Paxinos G, Watson C (2012) A multidimensional magnetic resonance histology atlas of the Wistar rat brain. Neuroimage 62(3): 1848–1856.

56. Veraart J, Leergaard TB, Antonsen BT, Van Hecke W, Blockx I, et al. (2011) Population-averaged diffusion tensor imaging atlas of the Sprague Dawley rat brain. Neuroimage 58: 975–983.

57. Hamano K, Iwasaki N, Takeya T, Takita H (1996) A quantitative analysis of rat central nervous system myelination using the immunohistochemical method for MBP. Brain Res Dev Brain Res 93: 18–22.

58. Pellicer F, Lopez-Avila A, Torres-Lopez E (1999) Electric stimulation of the cingulum bundle precipitates onset of autotomy induced by inflammation in rat. Eur J Pain 3: 287–293.

59. Barone FC, Wayner MJ, Scharoun SL, Guevara-Aguilar R, Aguilar-Baturoni HU (1981) Afferent connections to the lateral hypothalamus: a horseradish peroxidase study in the rat. Brain Res Bull 7: 75–88.

60. Giuditta M, Ruggiero DA, Del Bo A (2003) Anatomical basis for the fastigial pressor response. Blood Press 12: 175–180.

61. Kubicki M, Westin CF, Maier SE, Frumin M, Nestor PG, et al. (2002) Uncinate fasciculus findings in schizophrenia: a magnetic resonance diffusion tensor imaging study. Am J Psychiatry 159: 813–820.

62. Concha L, Gross DW, Wheatley BM, Beaulieu C (2006) Diffusion tensor imaging of time-dependent axonal and myelin degradation after corpus callosotomy in epilepsy patients. Neuroimage 32: 1090–1099.

63. DeBoy CA, Zhang J, Dike S, Shats I, Jones M, et al. (2007) High resolution diffusion tensor imaging of axonal damage in focal inflammatory and demyelinating lesions in rat spinal cord. Brain 130: 2199–2210.

64. Kim JH, Budde MD, Liang HF, Klein RS, Russell JH, et al. (2006) Detecting axon damage in spinal cord from a mouse model of multiple sclerosis. Neurobiol Dis 21: 626–632.

65. Schmierer K, Wheeler-Kingshott CA, Boulby PA, Scaravilli F, Altmann DR, et al. (2007) Diffusion tensor imaging of post mortem multiple sclerosis brain. Neuroimage 35: 467–477.

66. Fisher E, Chang A, Fox RJ, Tkach JA, Svarovsky T, et al. (2007) Imaging correlates of axonal swelling in chronic multiple sclerosis brains. Ann Neurol 62: 219–228.

67. Bozoki AC, Korolev IO, Davis NC, Hoisington LA, Berger KL (2011) Disruption of limbic white matter pathways in mild cognitive impairment and Alzheimer's disease: A DTI/FDG-PET Study. Hum Brain Mapp 33(8): 1792–1802.

68. Kampfl A, Franz G, Aichner F, Pfausler B, Haring HP, et al. (1998) The persistent vegetative state after closed head injury: clinical and magnetic resonance imaging findings in 42 patients. J Neurosurg 88: 809–816.

69. Batini C, Moruzzi G, Palestini M, Rossi GF, Zanchetti A (1958) Presistent patterns of wakefulness in the pretrigeminal midpontine preparation. Science 128: 30–32.

70. Parvizi J, Damasio AR (2003) Neuroanatomical correlates of brainstem coma. Brain 126: 1524–1536.

71. Sukhotinsky I, Zalkind V, Lu J, Hopkins DA, Saper CB, et al. (2007) Neural pathways associated with loss of consciousness caused by intracerebral microinjection of GABA A-active anesthetics. Eur J Neurosci 25: 1417–1436.

72. Franks NP (2008) General anaesthesia: from molecular targets to neuronal pathways of sleep and arousal. Nat Rev Neurosci 9: 370–386.

73. Hasenstaub A, Shu Y, Haider B, Kraushaar U, Duque A, et al. (2005) Inhibitory postsynaptic potentials carry synchronized frequency information in active cortical networks. Neuron 47: 423–435.

74. Llinas RR, Steriade M (2006) Bursting of thalamic neurons and states of vigilance. J Neurophysiol 95: 3297–3308.

75. Steriade M, McCormick DA, Sejnowski TJ (1993) Thalamocortical oscillations in the sleeping and aroused brain. Science 262: 679–685.

76. Lee MG, Manns ID, Alonso A, Jones BE (2004) Sleep-wake related discharge properties of basal forebrain neurons recorded with micropipettes in head-fixed rats. J Neurophysiol 92: 1182–1198.

77. Saper CB, Scammell TE, Lu J (2005) Hypothalamic regulation of sleep and circadian rhythms. Nature 437: 1257–1263.

78. Dringenberg HC, Olmstead MC (2003) Integrated contributions of basal forebrain and thalamus to neocortical activation elicited by pedunculopontine tegmental stimulation in urethane-anesthetized rats. Neuroscience 119: 839–853.

79. Starzl TE, Magoun HW (1951) Organization of the diffuse thalamic projection system. J Neurophysiol 14: 133–146.

80. Vanderwolf CH, Stewart DJ (1988) Thalamic control of neocortical activation: a critical re-evaluation. Brain Res Bull 20: 529–538.

81. Villablanca J, Salinas-Zeballos ME (1972) Sleep-wakefulness, EEG and behavioral studies of chronic cats without the thalamus: the 'athalamic' cat. Arch Ital Biol 110: 383–411.

82. Cape EG, Jones BE (2000) Effects of glutamate agonist versus procaine microinjections into the basal forebrain cholinergic cell area upon gamma and theta EEG activity and sleep-wake state. Eur J Neurosci 12: 2166–2184.

83. Buzsaki G, Bickford RG, Ponomareff G, Thal LJ, Mandel R, et al. (1988) Nucleus basalis and thalamic control of neocortical activity in the freely moving rat. J Neurosci 8: 4007–4026.

84. Kaur S, Junek A, Black MA, Semba K (2008) Effects of ibotenate and 192IgG-saporin lesions of the nucleus basalis magnocellularis/substantia innominata on spontaneous sleep and wake states and on recovery sleep after sleep deprivation in rats. J Neurosci 28: 491–504.

85. Fuller P, Sherman D, Pedersen NP, Saper CB, Lu J (2011) Reassessment of the structural basis of the ascending arousal system. J Comp Neurol 519: 933–956.

86. Jones BE (2005) From waking to sleeping: neuronal and chemical substrates. Trends Pharmacol Sci 26: 578–586.

87. Schwartz ML, Goldman-Rakic PS (1984) Callosal and intrahemispheric connectivity of the prefrontal association cortex in rhesus monkey: relation between intraparietal and principal sulcal cortex. J Comp Neurol 226: 403–420.

88. Soma S, Shimegi S, Osaki H, Sato H (2012) Cholinergic modulation of response gain in the primary visual cortex of the macaque. J Neurophysiol 107: 283–291.

89. Mrzljak L, Levey AI, Belcher S, Goldman-Rakic PS (1998) Localization of the m2 muscarinic acetylcholine receptor protein and mRNA in cortical neurons of the normal and cholinergically deafferented rhesus monkey. J Comp Neurol 390: 112–132.

90. Mrzljak L, Levey AI, Goldman-Rakic PS (1993) Association of m1 and m2 muscarinic receptor proteins with asymmetric synapses in the primate cerebral cortex: morphological evidence for cholinergic modulation of excitatory neurotransmission. Proc Natl Acad Sci U S A 90: 5194–5198.

91. Mrzljak L, Levey AI, Rakic P (1996) Selective expression of m2 muscarinic receptor in the parvocellular channel of the primate visual cortex. Proc Natl Acad Sci U S A 93: 7337–7340.

92. Mrzljak L, Pappy M, Leranth C, Goldman-Rakic PS (1995) Cholinergic synaptic circuitry in the macaque prefrontal cortex. J Comp Neurol 357: 603–617.

93. Agnati LF, Zoli M, Stromberg I, Fuxe K (1995) Intercellular communication in the brain: wiring versus volume transmission. Neuroscience 69: 711–726.

94. Bennett MR (1972) Autonomic neuromuscular transmission. Monogr Physiol Soc: 1–271.

95. Hulme EC, Birdsall NJ, Buckley NJ (1990) Muscarinic receptor subtypes. Annu Rev Pharmacol Toxicol 30: 633–673.

96. Metherate R, Tremblay N, Dykes RW (1987) Acetylcholine permits long-term enhancement of neuronal responsiveness in cat primary somatosensory cortex. Neuroscience 22: 75–81.

97. Tremblay N, Warren RA, Dykes RW (1990) Electrophysiological studies of acetylcholine and the role of the basal forebrain in the somatosensory cortex of the cat. II. Cortical neurons excited by somatic stimuli. J Neurophysiol 64: 1212–1222.

98. Massimini M, Ferrarelli F, Huber R, Esser SK, Singh H, et al. (2005) Breakdown of cortical effective connectivity during sleep. Science 309: 2228–2232.

99. Hobson JA, Pace-Schott EF, Stickgold R (2000) Dreaming and the brain: toward a cognitive neuroscience of conscious states. Behav Brain Sci 23: 793–842; discussion 904–1121.

100. Massimini M, Ferrarelli F, Murphy M, Huber R, Riedner B, et al. (2010) Cortical reactivity and effective connectivity during REM sleep in humans. Cogn Neurosci 1: 176–183.

101. Bennett MR (2011) Schizophrenia: susceptibility genes, dendritic-spine pathology and gray matter loss. Progress in Neurobiology 95(3): 275–300.

102. Soncrant TT, Horwitz B, Holloway HW, Rapoport SI (1986) The pattern of functional coupling of brain regions in the awake rat. Brain Res 369: 1–11.

103. Sokoloff L, Reivich M, Kennedy C, Des Rosiers MH, Patlak CS, et al. (1977) The [14C]deoxyglucose method for the measurement of local cerebral glucose utilization: theory, procedure, and normal values in the conscious and anesthetized albino rat. J Neurochem 28: 897–916.

104. Cavazzuti M, Porro C, Biral G, Benassi C, Barbieri G (1987) Ketamine effects onlocal cerebral blood flow and metabolism in the rat. J Cereb Blood Flow Metab 7: 806–811.

105. Gjedde A, Rasmussen M (1980) Pentobarbital anesthesia reduces blood-brain glucose transfer in the rat. J Neurochem 35: 1382–1387.

106. Toyama H, Ichise M, Liow JS, Modell KJ, Vines DC, et al. (2004) Absolute quantification of regional cerebral glucose utilization in mice by 18F-FDG small animal PET scanning and 2–14C-DG autoradiography. J Nucl Med 45: 1398–1405.

107. Nakao Y, Itoh Y, Kuang TY, Cook M, Jehle J, et al. (2001) Effects of anesthesia on functional activation of cerebral blood flow and metabolism. Proc Natl Acad Sci U S A 98: 7593–7598.

108. Eintrei C, Sokoloff L, Smith CB (1999) Effects of diazepam and ketamine administered individually or in combination on regional rates of glucose utilization in rat brain. Br J Anaesth 82: 596–602.

109. Crosby G, Crane AM, Sokoloff L (1982) Local changes in cerebral glucose utilization during ketamine anesthesia. Anesthesiology 56: 437–443.

110. Crosby G, Crane AM, Sokoloff L (1984) A comparison of local rates of glucose utilization in spinal cord and brain in conscious and nitrous oxide- or pentobarbital-treated rats. Anesthesiology 61: 434–438.

111. Redies C, Diksic M, Evans AC, Gjedde A, Yamamoto YL (1987) Double-label autoradiographic deoxyglucose method for sequential measurement of regional cerebral glucose utilization. Neuroscience 22: 601–619.

112. da Silva CG, Ribeiro CA, Leipnitz G, Dutra-Filho CS, Wyse AA, et al. (2002) Inhibition of cytochrome c oxidase activity in rat cerebral cortex and human skeletal muscle by D-2-hydroxyglutaric acid in vitro. Biochim Biophys Acta 1586: 81–91.

113. Suarez RK, Doll CJ, Buie AE, West TG, Funk GD, et al. (1989) Turtles and rats: a biochemical comparison of anoxia-tolerant and anoxia-sensitive brains. Am J Physiol 257: R1083–1088.

114. Steinberg JL, Devous MD Sr, Moeller FG, Paulman RG, Raese JD, et al. (1995) Cerebellar blood flow in schizophrenic patients and normal control subjects. Psychiatry Res 61: 15–31.

115. Newman GC, Hospod FE, Maghsoudlou B, Patlak CS (1996) Simplified brain slice glucose utilization. J Cereb Blood Flow Metab 16: 864–880.

116. Newman GC, Hospod FE, Wu P (1989) Glucose utilization of ischemic hippocampal slices. J Neurosci Methods 28: 23–34.

117. Newman GC, Hospod FE, Schissel SL (1991) Ischemic brain slice glucose utilization: effects of slice thickness, acidosis, and K+. J Cereb Blood Flow Metab 11: 398–406.

118. Newman GC, Hospod FE, Wu P (1988) Thick brain slices model the ischemic penumbra. J Cereb Blood Flow Metab 8: 586–597.

119. Newman GC, Hospod FE, Patlak CS, Moore RY (1992) Analysis of in vitro glucose utilization in a circadian pacemaker model. J Neurosci 12: 2015–2021.

120. Shibata S, Newman GC, Moore RY (1987) Effects of calcium ions on glucose utilization in the rat suprachiasmatic nucleus in vitro. Brain Res 426: 332–338.

121. Shibata S, Moore RY (1988) Electrical and metabolic activity of suprachiasmatic nucleus neurons in hamster hypothalamic slices. Brain Res 438: 374–378.

122. Rolleston FS, Newsholme EA (1967) Effects of fatty acids, ketone bodies, lactate and pyruvate on glucose utilization by guinea-pig cerebral cortex slices. Biochem J 104: 519–523.

123. Otsuka T, Wei L, Acuff VR, Shimizu A, Pettigrew KD, et al. (1991) Variation in local cerebral blood flow response to high-dose pentobarbital sodium in the rat. Am J Physiol 261: H110–120.

124. Hayashi T, Fukuyama H, Katsumi Y, Hanakawa T, Nagahama Y, et al. (1999) Cerebral glucose metabolism in unilateral entorhinal cortex-lesioned rats: an animal PET study. Neuroreport 10: 2113–2118.

125. Heiss WD, Pawlik G, Herholz K, Wagner R, Wienhard K (1985) Regional cerebral glucose metabolism in man during wakefulness, sleep, and dreaming. Brain Res 327: 362–366.

126. Alkire MT, Haier RJ, Barker SJ, Shah NK, Wu JC, et al. (1995) Cerebral metabolism during propofol anesthesia in humans studied with positron emission tomography. Anesthesiology 82: 393–403; discussion 327A.

127. Shen J, Petersen KF, Behar KL, Brown P, Nixon TW, et al. (1999) Determination of the rate of the glutamate/glutamine cycle in the human brain by in vivo 13C NMR. Proc Natl Acad Sci U S A 96: 8235–8240.

128. Pan JW, Rothman TL, Behar KL, Stein DT, Hetherington HP (2000) Human brain beta-hydroxybutyrate and lactate increase in fasting-induced ketosis. J Cereb Blood Flow Metab 20: 1502–1507.

129. Chen W, Zhu XH, Gruetter R, Seaquist ER, Adriany G, et al. (2001) Study of tricarboxylic acid cycle flux changes in human visual cortex during hemifield visual stimulation using (1)H-[(13)C] MRS and fMRI. Magn Reson Med 45: 349–355.

130. Chhina N, Kuestermann E, Halliday J, Simpson LJ, Macdonald IA, et al. (2001) Measurement of human tricarboxylic acid cycle rates during visual activation by (13)C magnetic resonance spectroscopy. J Neurosci Res 66: 737–746.

131. Gruetter R, Seaquist ER, Ugurbil K (2001) A mathematical model of compartmentalized neurotransmitter metabolism in the human brain. Am J Physiol Endocrinol Metab 281: E100–112.

132. Lebon V, Petersen KF, Cline GW, Shen J, Mason GF, et al. (2002) Astroglial contribution to brain energy metabolism in humans revealed by 13C nuclear magnetic resonance spectroscopy: elucidation of the dominant pathway for neurotransmitter glutamate repletion and measurement of astrocytic oxidative metabolism. J Neurosci 22: 1523–1531.

133. Gruetter R (2002) In vivo 13C NMR studies of compartmentalized cerebral carbohydrate metabolism. Neurochem Int 41: 143–154.

134. Mason GF, Petersen KF, de Graaf RA, Shulman GI, Rothman DL (2007) Measurements of the anaplerotic rate in the human cerebral cortex using 13C magnetic resonance spectroscopy and [1–13C] and [2–13C] glucose. J Neurochem 100: 73–86.

135. Boumezbeur F, Mason GF, de Graaf RA, Behar KL, Cline GW, et al. (2010) Altered brain mitochondrial metabolism in healthy aging as assessed by in vivo magnetic resonance spectroscopy. J Cereb Blood Flow Metab 30: 211–221.

136. Kaisti KK, Langsjo JW, Aalto S, Oikonen V, Sipila H, et al. (2003) Effects of sevoflurane, propofol, and adjunct nitrous oxide on regional cerebral blood flow, oxygen consumption, and blood volume in humans. Anesthesiology 99: 603–613.

137. Alkire MT, Pomfrett CJ, Haier RJ, Gianzero MV, Chan CM, et al. (1999) Functional brain imaging during anesthesia in humans: effects of halothane on global and regional cerebral glucose metabolism. Anesthesiology 90: 701–709.

138. Schlunzen L, Vafaee MS, Juul N, Cold GE (2010) Regional cerebral blood flow responses to hyperventilation during sevoflurane anaesthesia studied with PET. Acta Anaesthesiol Scand 54: 610–615.

139. Seok JH, Park HJ, Chun JW, Lee SK, Cho HS, et al. (2007) White matter abnormalities associated with auditory hallucinations in schizophrenia: a combined study of voxel-based analyses of diffusion tensor imaging and structural magnetic resonance imaging. Psychiatry Res 156: 93–104.

140. Rowland LM, Spieker EA, Francis A, Barker PB, Carpenter WT, et al. (2009) White matter alterations in deficit schizophrenia. Neuropsychopharmacology 34: 1514–1522.

141. Szeszko PR, Ardekani BA, Ashtari M, Kumra S, Robinson DG, et al. (2005) White matter abnormalities in first-episode schizophrenia or schizoaffective disorder: a diffusion tensor imaging study. Am J Psychiatry 162: 602–605.

142. Federspiel A, Begre S, Kiefer C, Schroth G, Strik WK, et al. (2006) Alterations of white matter connectivity in first episode schizophrenia. Neurobiol Dis 22: 702–709.

143. Buchsbaum MS, Ingvar DH, Kessler R, Waters RN, Cappelletti J, et al. (1982) Cerebral glucography with positron tomography. Use in normal subjects and in patients with schizophrenia. Arch Gen Psychiatry 39: 251–259.

144. Wolkin A, Sanfilipo M, Angrist B, Duncan E, Wieland S, et al. (1994) Acute d-amphetamine challenge in schizophrenia: effects on cerebral glucose utilization and clinical symptomatology. Biol Psychiatry 36: 317–325.

145. Kling AS, Metter EJ, Riege WH, Kuhl DE (1986) Comparison of PET measurement of local brain glucose metabolism and CAT measurement of brain atrophy in chronic schizophrenia and depression. Am J Psychiatry 143: 175–180.

146. al-Mousawi AH, Evans N, Ebmeier KP, Roeda D, Chaloner F, et al. (1996) Limbic dysfunction in schizophrenia and mania. A study using 18F-labelled fluorodeoxyglucose and positron emission tomography. Br J Psychiatry 169: 509–516.

147. Biver F, Goldman S, Luxen A, Delvenne V, De Maertelaer V, et al. (1995) Altered frontostriatal relationship in unmedicated schizophrenic patients. Psychiatry Res 61: 161–171.

148. Weinberger DR, Berman KF, Zec RF (1986) Physiologic dysfunction of dorsolateral prefrontal cortex in schizophrenia. I. Regional cerebral blood flow evidence. Arch Gen Psychiatry 43: 114–124.

149. Gur RE, Resnick SM, Gur RC, Alavi A, Caroff S, et al. (1987) Regional brain function in schizophrenia. II. Repeated evaluation with positron emission tomography. Arch Gen Psychiatry 44: 126–129.

150. DeLisi LE, Holcomb HH, Cohen RM, Pickar D, Carpenter W, et al. (1985) Positron emission tomography in schizophrenic patients with and without neuroleptic medication. J Cereb Blood Flow Metab 5: 201–206.

151. Siegel BV Jr, Buchsbaum MS, Bunney WE Jr, Gottschalk LA, Haier RJ, et al. (1993) Cortical-striatal-thalamic circuits and brain glucose metabolic activity in 70 unmedicated male schizophrenic patients. Am J Psychiatry 150: 1325–1336.

152. Farkas T, Wolf AP, Jaeger J, Brodie JD, Christman DR, et al. (1984) Regional brain glucose metabolism in chronic schizophrenia. A positron emission transaxial tomographic study. Arch Gen Psychiatry 41: 293–300.

153. Fujimoto T, Takeuch K, Matsumoto T, Kamimura K, Hamada R, et al. (2007) Abnormal glucose metabolism in the anterior cingulate cortex in patients with schizophrenia. Psychiatry Res 154: 49–58.

154. Buchsbaum MS, Someya T, Teng CY, Abel L, Chin S, et al. (1996) PET and MRI of the thalamus in never-medicated patients with schizophrenia. Am J Psychiatry 153: 191–199.

155. Hazlett EA, Buchsbaum MS, Kemether E, Bloom R, Platholi J, et al. (2004) Abnormal glucose metabolism in the mediodorsal nucleus of the thalamus in schizophrenia. Am J Psychiatry 161: 305–314.

156. Resnick SM, Gur RE, Alavi A, Gur RC, Reivich M (1988) Positron emission tomography and subcortical glucose metabolism in schizophrenia. Psychiatry Res 24: 1–11.

157. Vita A, Dieci M, Giobbio GM, Garbarini M, Morganti C, et al. (1994) A reconsideration of the relationship between cerebral structural abnormalities and family history of schizophrenia. Psychiatry Res 53: 41–55.

158. Rubin P, Holm S, Madsen PL, Friberg L, Videbech P, et al. (1994) Regional cerebral blood flow distribution in newly diagnosed schizophrenia and schizophreniform disorder. Psychiatry Res 53: 57–75.

159. Sachdev P, Brodaty H, Rose N, Haindl W (1997) Regional cerebral blood flow in late-onset schizophrenia: a SPECT study using 99mTc-HMPAO. Schizophr Res 27: 105–117.

160. Scottish Schizophrenia Research Group (1998) Regional cerebral blood flow in first-episode schizophrenia patients before and after antipsychotic drug treatment. Acta Psychiatr Scand 97: 440–449.

161. Parellada E, Catafau AM, Bernardo M, Lomena F, Catarineu S, et al. (1998) The resting and activation issue of hypofrontality: a single photon emission computed tomography study in neuroleptic-naive and neuroleptic-free schizophrenic female patients. Biol Psychiatry 44: 787–790.

162. Parellada E, Catafau AM, Bernardo M, Lomena F, Gonzalez-Monclus E, et al. (1994) Prefrontal dysfunction in young acute neuroleptic-naive schizophrenia patients: a resting and activation SPECT study. Psychiatry Research 55: 131–139.

163. Soyka M, Koch W, Moller HJ, Ruther T, Tatsch K (2005) Hypermetabolic pattern in frontal cortex and other brain regions in unmedicated schizophrenia patients. Results from a FDG-PET study. Eur Arch Psychiatry Clin Neurosci 255: 308–312.